CIVIL ENGINEERING JOURNAL

Article no. 23

THE CIVIL ENGINEERING JOURNAL 3-2024

SEISMIC INVESTIGATION OF STRENGTHENED SOIL WALLS WITH GEOGRIDS

Hongliang Yue and Xiaoyong Liang

School of Civil Engineering, Hebei University of Science and Technology, Shijiazhuang, 050018, China; lxy063019@163.com

ABSTRACT

This study explores the impact of various factors on the seismic behavior of geogrid-strengthened soil walls. The research involves modifying soil properties like friction angle, cohesion, elastic modulus, and Poisson's ratio. The aim is to comprehend the consequent effects on the wall's horizontal and vertical deformations, the lateral pressure applied to the wall's surface, and the peak pulling force encountered by strengthening under seismic states with a maximum acceleration of 0.3 g. The primary goal is to boost the seismic execution of such walls and analogous scenarios. To attain this goal, a two-dimensional numerical analysis is performed employing the finite difference method and FLAC software while accounting for strain considerations. The analysis findings reveal that increasing cohesion at the wall's height results in a nearly consistent peak pulling force on the reinforcements. However, the impact of cohesion on this force diminishes for wall heights exceeding 4 meters. Elevating the internal friction angle leads to a reduction in the peak pulling force on the reinforcements, particularly in the lower segment of the wall. Conversely, with increasing wall height, the decrease in horizontal pressure on the wall's rear surface becomes less noticeable, eventually stabilizing at around 1 kilopascal in the upper half of the wall. Altering the soil's elastic modulus demonstrates that once the value surpasses 35 MPa, the peak pulling force on the reinforcements remains stable, exhibiting no further alterations.

KEYWORDS

Strengthened soil walls, Seismic analysis, FLAC numerical pattern, Finite difference method, Deformation, Soil cohesion, Soil friction angle

INTRODUCTION

Strengthened soil walls have historically played a pivotal role in the evolution of geotechnical engineering. Their economical construction costs, minimal settlement, and effective resistance against seismic loads make them crucial subjects of study (Bao et al., 2023; Nunes et al., 2022). Presently, these structures are referred to as Mechanically Stabilized Earth Walls (MSEW) (Huang, 2019; Xu et al., 2020; Yang et al., 2023). The United States began employing strengthened soil techniques for retaining wall construction around 1972. Notably, more than 7,000 such walls were built between 1972 and 1996, with over 200,000 structures executed globally in the past two decades in 11 diverse countries (Bathurst & Hatami, 1998).

Initially, metal straps were used for wall reinforcement, later replaced by welded wire mesh. These frameworks faced issues such as susceptibility to corrosion and high costs. Consequently, the emergence of polymer geosynthetics offered an economically viable and corrosion-resistant solution. These geosynthetics are grouped into categories, including geotextiles, geogrids, geonets, and geocomposites. Geotextiles and geogrids are commonly used for soil reinforcement and

contribute to stability through functions like filtration, drainage, and separation (Changizi et al., 2022; Geng, 2021).

The introduction of geotextile reinforcement took place in France in 1972, marking a turning point in geotextile use for soil reinforcement, especially since the 1980s. Geogrids similarly gained prominence in this period and currently maintain a significant market presence (Holtz, 2017). Notably, geosynthetics exhibit superior tensile strength compared to metals, albeit with higher deformation. Additionally, geosynthetics display distinctive long-term behavior due to gradual "creep," causing increased deformation over time (Leshchinsky & Han, 2004).

Numerical studies on strengthened soil structures were historically limited due to information gaps and skepticism regarding numerical frameworks. However, recent years have witnessed a growing recognition of the potential of these frameworks. For instance, Cai and Bathurst (1995) utilized modified TARA-3 software to simulate earthquake-resistant walls with segmented geosynthetic facades. They employed the El Centro (1940) earthquake acceleration curve, applying maximum values of 0.125 and 0.25 g at a reduced scale. Segrestin and Bastick (1988) utilized the SUPER FLUSH finite element program, obtaining promising outcomes comparable to shake table tests. More recently, researchers like Zhang et al. (2020), Ling (2023), Ren et al. (2024), and Majumder et al. (2023) have delved into various aspects of numerical analysis to understand the seismic response and behavior of strengthened soil walls under various states (Fairless, 1989; Javdanian & Goudarzi, 2023; Murali Krishna & Madhavi Latha, 2009; Qian, 2023; Safaee et al., 2023; Zhou & Ding, 2021).

Despite these advances, laboratory investigations of diverse parameters, particularly under seismic states, pose challenges due to complexity and costs. Consequently, numerical frameworks offer an efficient alternative, providing detailed outcomes for accurate execution assessment and model validation. However, in the context of strengthened soil, few instances of actual earthquake-condition model outcomes can be found in the technical literature. To ensure numerical accuracy, comparisons were drawn between a one-meter-high instrumented laboratory model and a constructed seven-meter-high model subjected to earthquake loads in FLAC software. This study aims to contribute to understanding seismic behavior through the comparison and evaluation of constructed numerical frameworks against laboratory cases, emphasizing novel insights into the reaction of stabilized soil walls under seismic states.

NUMERICAL PATTERN

In this study, the impactiveness of the FLAC software's execution is evaluated by comparing outcomes derived from a numerical pattern generated through this software with those obtained from an analogous model subjected to laboratory experimentation. To validate the precision of the FLAC software under seismic states, a series of shake table experiments carried out by Bathurst and his associates at the Royal Military College (RMC) in Canada were utilized. These tests were conducted using a one-meter-scale design of a stabilized soil geosynthetic wall with a continuous facade, based on the structure proposed by Iai (1989). To faithfully replicate states resembling real-world scenarios, meticulous attention was given to factors such as the wall's physical dimensions, soil characteristics, and stiffness of the geosynthetic reinforcement. A visual representation of this wall's geometry on the shake table is depicted in Figure 1.

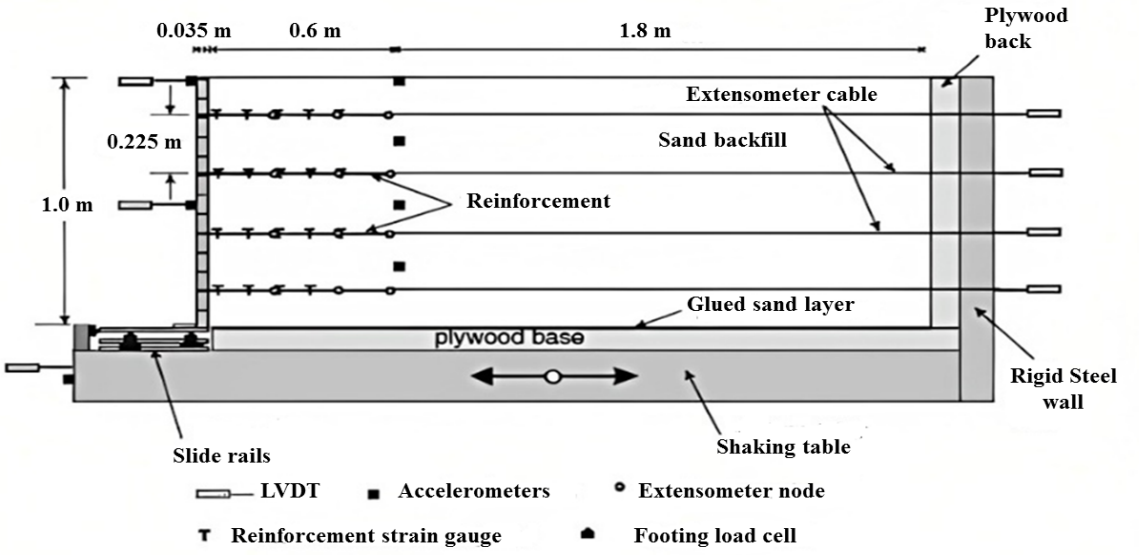

Fig.1- Wall-mounted tool model on a shaky table

A 5 Hz frequency wave with a constant amplitude every 5 seconds has been used to shake the wall to demonstrate it, as displayed in Figure 2

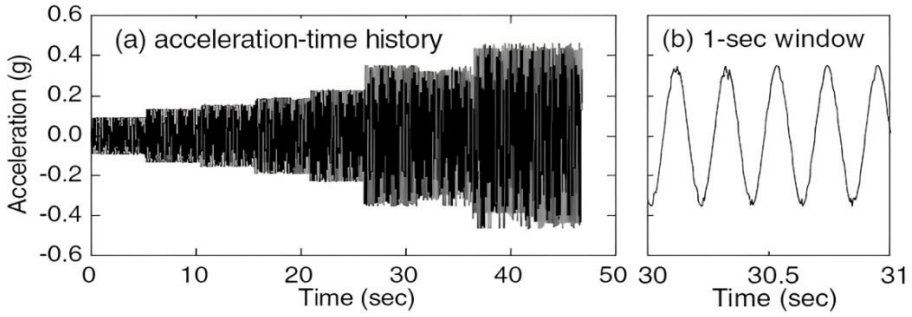

Fig. 2 - The base acceleration is used in the shaky table model.

Figure 3 depicts the finite difference model generated through FLAC, representing the RMC vibration table. The wall was composed of soil with a specific weight of 15.7 KN/m³, an inner friction angle of 46 degrees, a bulk modulus (K) of 6 MPa, and a shear modulus (G) of 7 MPa. For wall strengthening, a geogrid with a tensile strength (Tu) of 13 MPa, flexural strength (Tf) of 6.5 MPa, and an elasticity modulus (E) of 45 MPa was utilized. The behavioral model applied to both the strengthened soil and retained soil adheres to the principles of Mohr-Coulomb.

To ensure proper meshing of the model and alignment of existing zones with wave propagation states, equations from the Coulomb-Lee model were employed.

$$Cs = \sqrt{\frac{G}{\rho}} = 104 \;\; \Delta l \le \frac{Cs}{10\,f} = 2.1 \tag{1}$$

In Equation 1, Cs represents the shear wave velocity, G is the shear modulus, ρ denotes the density of the material, and f stands for the natural frequency of the soil layer. The modeling process imposes a maximum zone size limit of 2.1 meters. Therefore, constructing the model requires a mesh size smaller than this threshold. To ensure the accuracy of the results, mesh sizes of 0.1, 0.5,

and 1 meter were evaluated. The analysis runtime for a 0.1-meter mesh size exceeded 24 hours, which is the upper time limit. Similar outcomes were observed for the 0.5 and 1-meter mesh sizes.

Consequently, due to the impractical duration required for a 0.5-meter mesh model, a 1-meter mesh size was adopted for the intended model. The base soil and wall frontage were modeled with elastic frameworks. Cable elements were used to represent the reinforcements, while the interactions among the base and retaining soil, the frontage and retaining soil, and the retaining soil and interface element were simulated. An interface element was included to simulate the wall's foundation, enabling sliding states, simultaneous rotation, and displacement by assigning an internal friction angle of zero. The input wave used in FLAC is visualized in Figure 3.

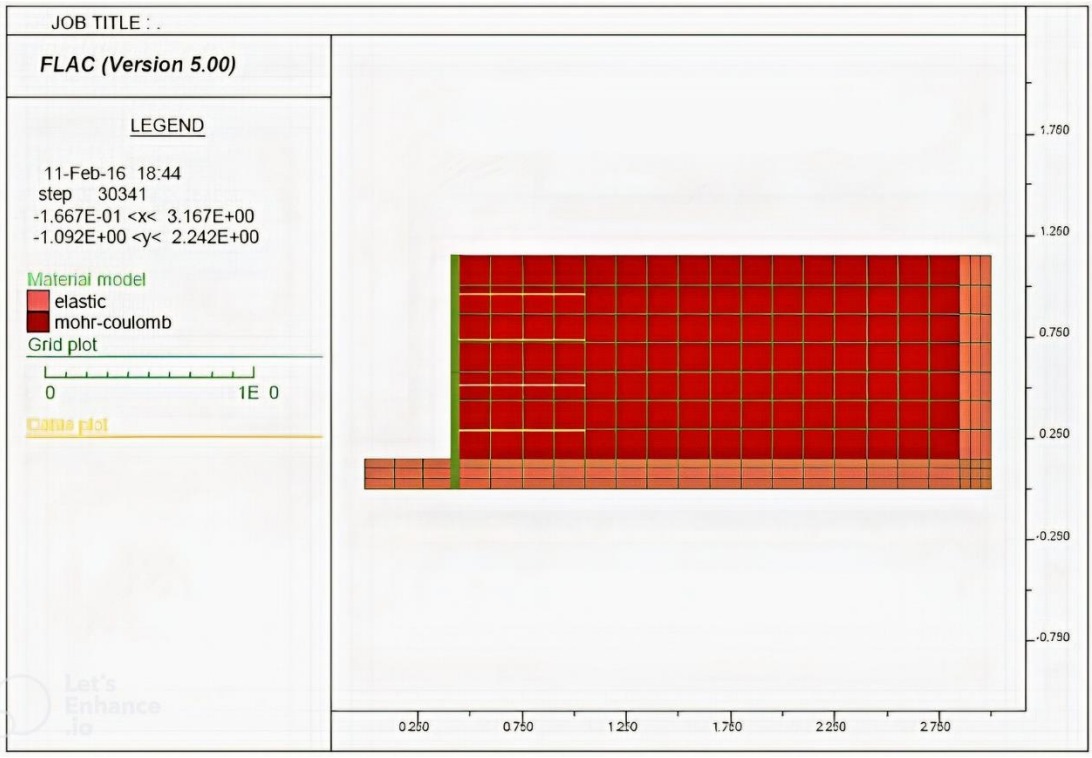

Fig. 3 - The finite difference mesh of the vibration table model

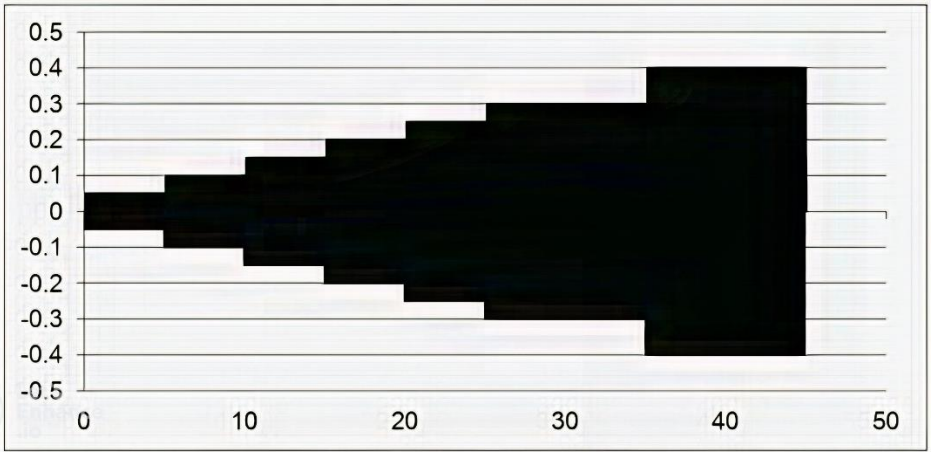

Fig. 4 - The base acceleration is used in the FLAC model.

In Figure 4, the term "base acceleration" refers to the fundamental level of acceleration integrated into the FLAC model. This essential parameter plays a crucial role in governing the

model's response and behavior during simulations. It serves as a foundational input that impacts various aspects of the model's dynamics and outcomes. By defining the base acceleration, the model can precisely simulate and analyze how structures or materials respond under diverse seismic states or loading scenarios. This ensures accuracy in predicting and comprehending the execution and stability of engineered systems under seismic forces.

Figure 5 displays that the FLAC outcomes demonstrate relatively good consistency with the measured parameters. As depicted in the figure, significant values are observed following a horizontal shift of the facade. The base acceleration utilized was 0.3 g.

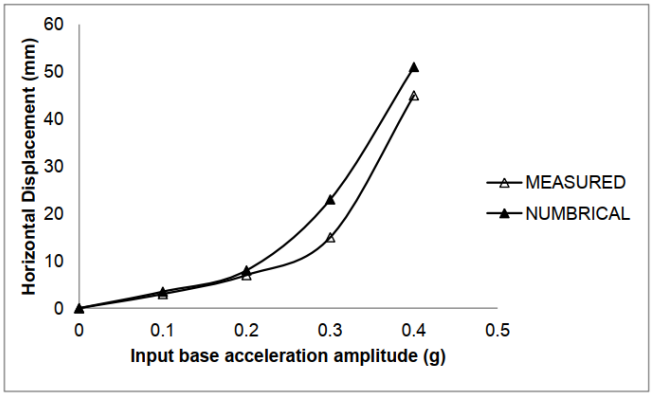

Fig. 5 - Estimated and quantified horizontal shift of the top of the wall against input acceleration.

Tab. 1 - Summary of the parameters

Parameter	Value/Description
Seismic Acceleration	0.3 g
Soil Properties	
Friction Angle (φ)	34 º, 39 º, 44 º, 49º
Elastic Modulus (E)	20, 35, 50, 60 MPa
Poisson's Ratio (PR)	0.25, 0.3, 0.65
Reinforcement Properties	Geogrid

In this study, the following parameters were analyzed to evaluate the seismic behavior of geogrid-strengthened soil walls: The friction angle (φ) values were set at 34°, 39°, 44°, and 49° to explore the impact of soil shear strength on the wall's execution. The elastic modulus (E) values were varied at 20, 35, 50, and 60 MPa to assess how changes in soil stiffness influence the deformations and forces within the wall structure. Additionally, Poisson's ratio (PR) was considered at values of 0.25, 0.3, and 0.65 to understand its impact on the soil behavior under seismic loading. These parameters were systematically varied to comprehensively understand their effects on horizontal and vertical deformations, the lateral pressure exerted on the wall, and the peak pulling forces endured by the geogrid strengthening. The study aimed to offer robust insights into optimizing the structure and execution of geogrid-strengthened soil walls under seismic states by incorporating a range of values for these critical parameters.

OUTCOMES AND DISCUSSION

Boundary States and Model Loading Under Seismic States: In this scenario, a sole horizontal seismic loading element is employed to the lowermost points of the model. This acceleration is

introduced when the system reaches a state of static equilibrium, with all point displacements held at zero (Sadighi et al., 2022). Consequently, the displacements witnessed during the seismic analysis are exclusively attributed to the impact of seismic loads. It's crucial to acknowledge that forces derived from combined static and seismic analyses deviate from those originating solely from static analysis. This deviation arises due to the persistence of forces, despite setting displacements to zero. Figure 6 depicts the 0.3 g acceleration utilized in the context of the discussed wall model.

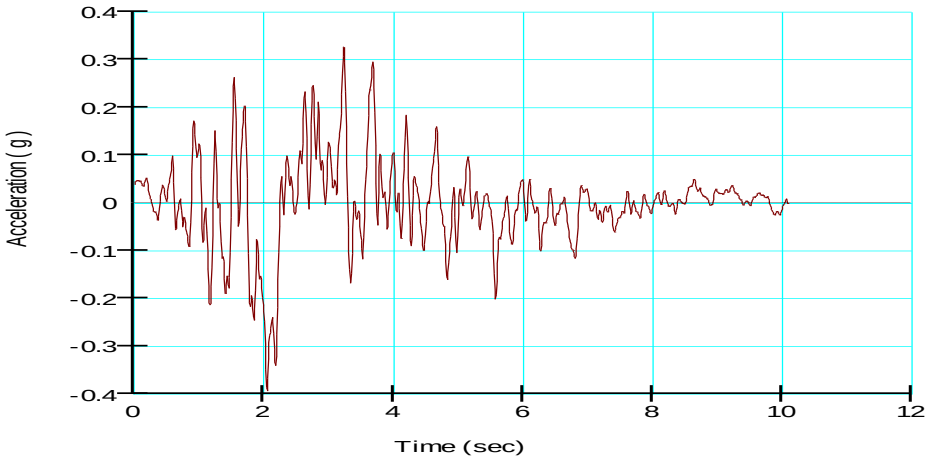

Fig. 6 - The input wave in the seismic analysis of the numerical pattern for the strengthened soil wall

Parametric Study on Strengthened soil Wall under Seismic States

Subjecting the strengthened soil wall to seismic loading aims to investigate factors influencing its stability and the extent of its deformations. As part of this study, modifications have been implemented in the properties of the strengthened soil to assess their impact on the structure's behavior.

Findings with Fundamental Soil Properties: This segment centers on the strengthened soil wall with basic soil attributes—C=0, v=0.3, E=35 MPa, and φ=34. The wall is exposed to a maximum speed gain of 0.3 g, and its conduct is observed under static and seismic scenarios.

A) Peak Pulling force of Reinforcements:

Figure 7 portrays alterations in the highest pulling force of reinforcements under static and seismic states, along with the total force. From the visual representation, it can be deduced that heightened pulling force within reinforcements primarily transpires in the lower portion of the wall, particularly at its base. This trend can be attributed to the augmented seismic loading, which significantly influences the reaction of the lower segment of the wall.

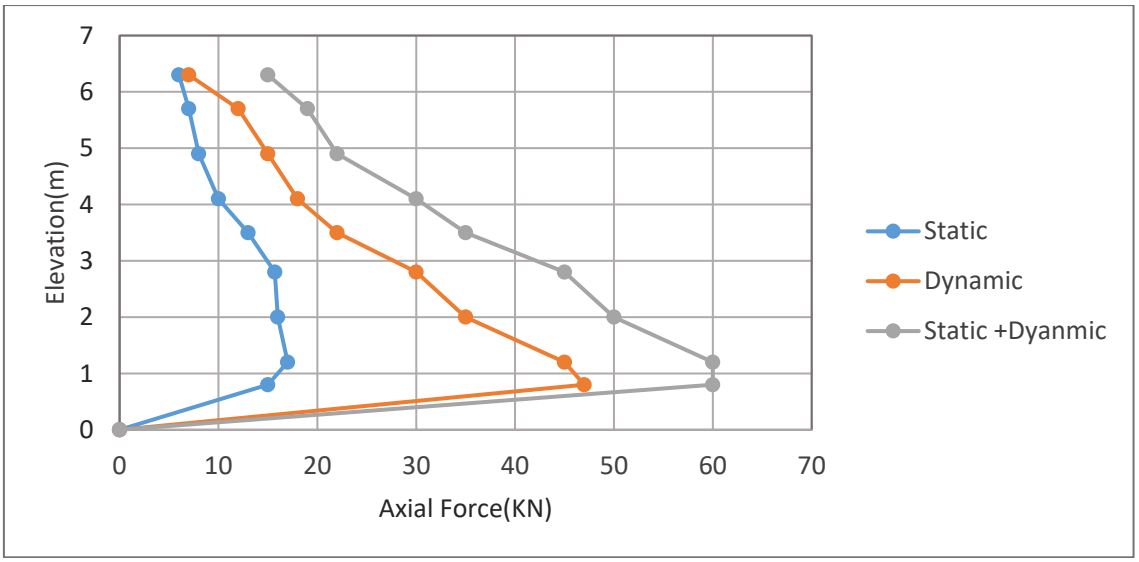

Fig. 7 - The highest pulling force of reinforcements with basic soil properties under static and seismic states at the end of the 0.3 g base acceleration

B) Horizontal Pressure on the Rear of the Wall:

Figure 8 illustrates the alterations in the horizontal pressure exerted on the rear side, considering basic soil characteristics under both static and seismic states. Notably, in seismic states, the horizontal pressure on the wall's rear side undergoes a more substantial augmentation in the lower half compared to the upper portion. This observation highlights that the impact of seismic loading is more pronounced in the lower segment of the wall. This phenomenon can be assigned to the increased weight and subsequent rise in lateral pressure at greater depths, particularly in seismic scenarios.

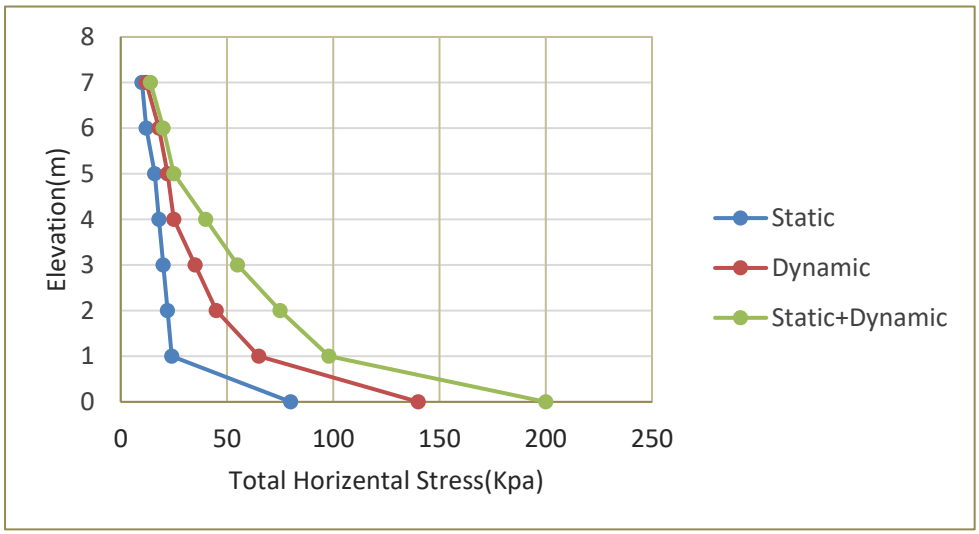

Fig. 8 - Horizontal pressure on the rear of the wall with basic soil properties under static and at the end of the 0.3 g base acceleration

C) Horizontal shift of the Wall:

Figure 9 presents the horizontal shifts of the wall relative to its height under static and seismic states. Evidently, the magnitude of horizontal shifts is amplified fourfold under seismic states in

comparison to static states. This stark contrast underscores the substantial impact of seismic activity on the wall's behavior.

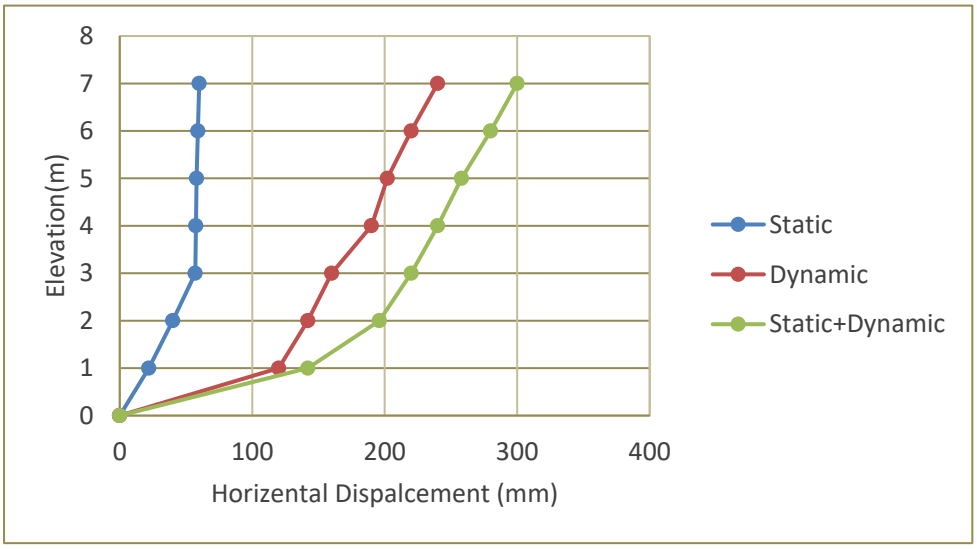

Fig. 9 - Horizontal shifts of the wall with basic soil properties under static and at the end of the 0.3 g base acceleration

The impact of the Internal Friction Angle of Strengthened soil on the Response of the Structure

Within this segment, the structure's response is explored across various internal friction angle values of the strengthened soil. Throughout all analyses, cohesion is presumed to be absent, and a maximum acceleration of 0.3 g is employed to the system.

A) Peak Pulling force of Reinforcements:

Figure 10 portrays the impact of the internal friction angle on the peak pulling force experienced by the reinforcements. Notably, as it escalates, the highest pulling force of the reinforcements diminishes, particularly in the lower section of the wall. With escalating φ values, the curves within Figure 10 converge, indicating a trend toward similarity.

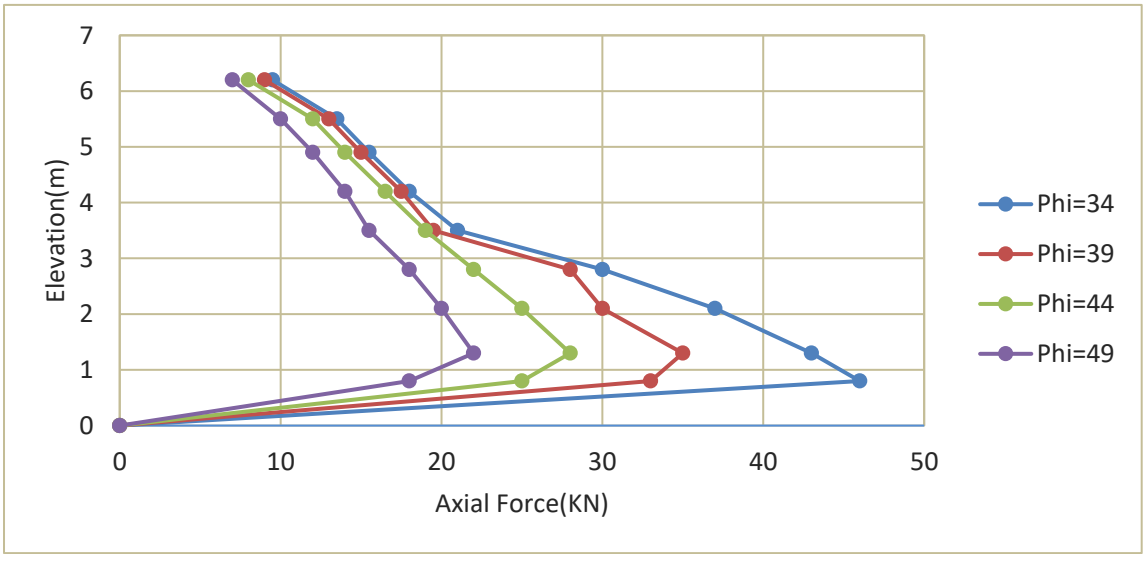

B) Horizontal Pressure on the Wall's Rear Surface

Figure 11 illustrates the shifts in horizontal pressure on the wall's rear surface. The pressure diminishes as the internal friction angle of the strengthened soil rises. This decrease is especially prominent in the wall's lower half. With increasing height, the magnitude of this reduction wanes, eventually stabilizing at around 1 kPa in the upper portion of the wall. It's noteworthy that the spacing between the curves remains uniform as the φ value increases.

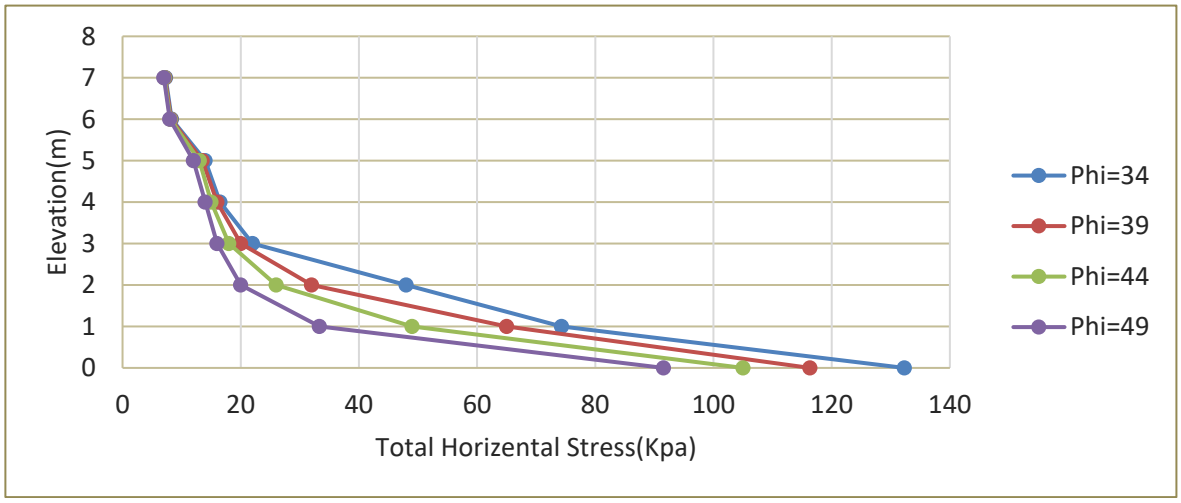

Fig. 11 - The impact of the internal friction angle of the strengthened soil on the horizontal pressure exerted on the rear of the wall at the conclusion of the 0.3 g base input acceleration

C) Horizontal shift of the Wall:

Figure 12 displays the trend of horizontal shifts with increasing internal friction angle. As observed, increasing φ leads to a reduction in the magnitude of horizontal shifts of the wall. The distance between the curves becomes less than the other curves for φ≥39°.

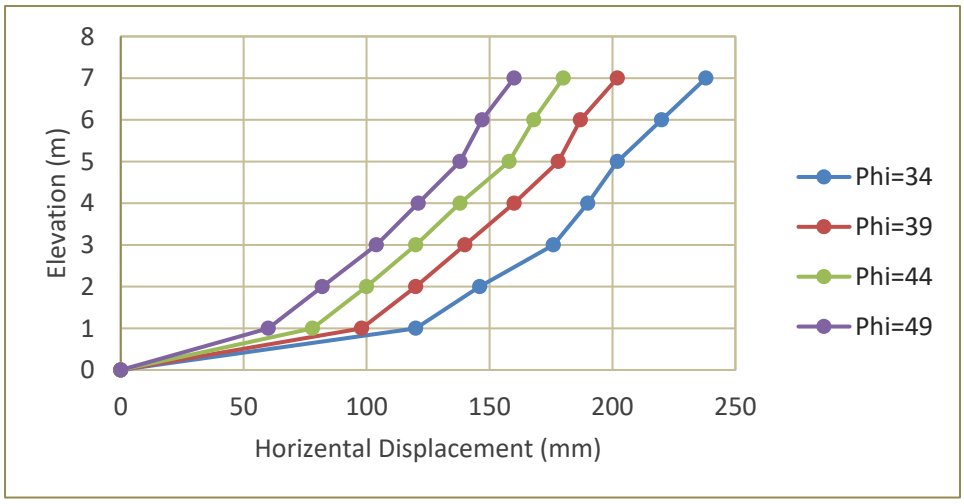

Fig. 12 - Effect of the internal friction angle of the strengthened soil on the horizontal shift of the wall at the end of the 0.3 g base input acceleration

D) Vertical shift of the Top and Bottom of the Wall:

Figure 13 displays that increasing the internal friction angle results in a reduction in the vertical shifts of the top and bottom of the wall.

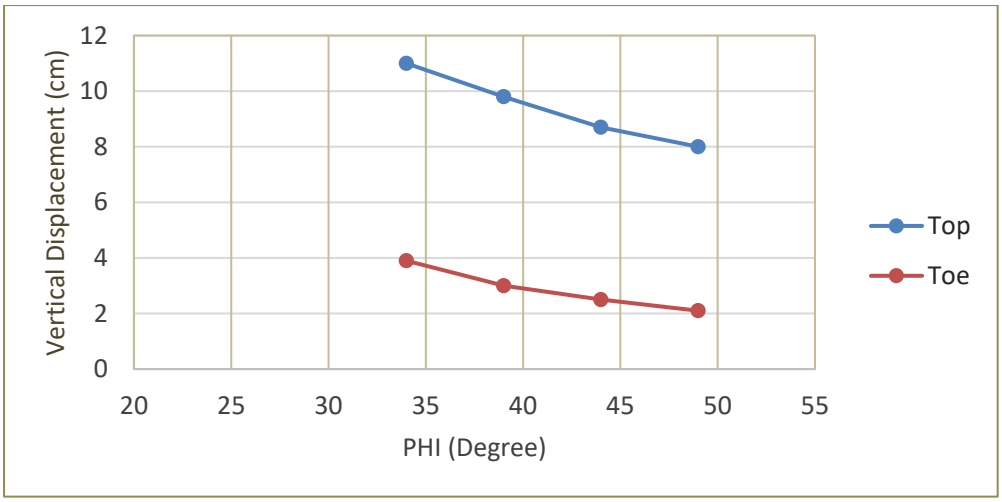

Fig. 13 - Effect of the internal friction angle of the strengthened soil on the vertical shifts of the top and bottom of the wall at the end of the 0.3 g base input acceleration

The impact of the Elastic Modulus of the Strengthened soil on the Reaction of the Structure

In this section, the structural behavior is assessed through the manipulation of the strengthened soil's elastic modulus, ranging from 20 to 60 kPa. The repercussions of this variability are explored. It's important to highlight that across all analyses, the internal friction angle and cohesion remain constant at 34 and 0 degrees, respectively. Furthermore, a uniform maximum acceleration of 0.3 g is incorporated in all scenarios.

A) Peak Pulling force of Reinforcements:

Figure 14 visualizes the alteration in the peak pulling force endured by the reinforcements concerning height, considering diverse elastic modulus values for the strengthened soil (ES). Notably, these curves demonstrate that when the elastic modulus of the strengthened soil (ES) surpasses 35 MPa, the highest pulling force within the reinforcements stabilizes at a constant value, signifying the absence of further fluctuations.

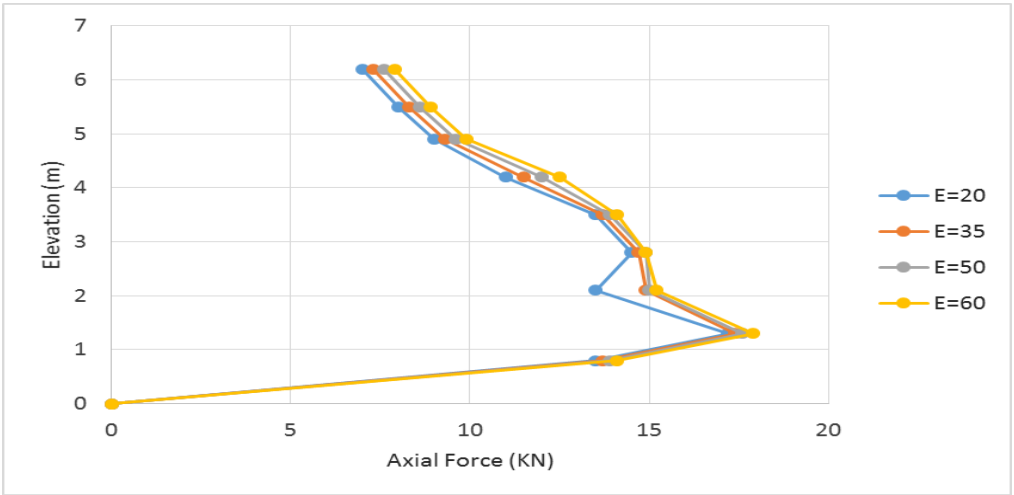

Fig. 14 - Effect of the elastic modulus of the strengthened soil on the highest pulling force of reinforcements at the end of the 0.3 g base input acceleration

B) Horizontal Pressure on the Rear of the Wall:

The changes in horizontal pressure on the wall's rear surface, corresponding to the rising elastic modulus of the strengthened soil, are illustrated in Fig. 15. When the elastic modulus (ES) elevates from 20 to 35 MPa, a decline in the horizontal pressure on the wall's rear side becomes evident. The bottom point of the wall manifests the most substantial reduction, amounting to 11.6 kPa. However, for ES values equal to or exceeding 35 MPa, notable shifts in horizontal pressure on the wall's rear surface are not discernible.

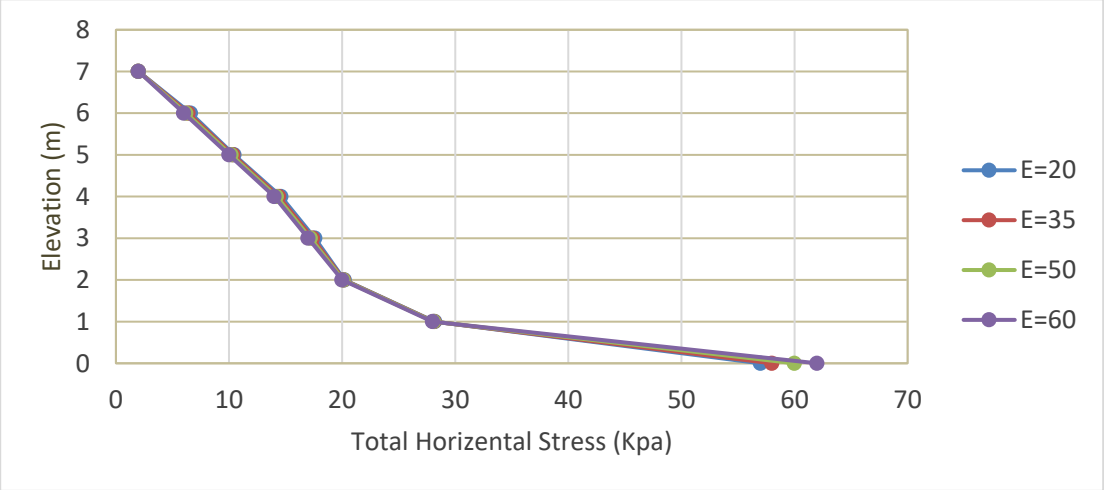

Fig. 15 - Effect of the elastic modulus of the strengthened soil on the horizontal pressure on the rear of the wall at the end of the 0.3 g base input acceleration

C) Horizontal shift of the Wall:

Figure 16 displays the variation of horizontal shifts of the wall with height for diverse values of the elastic modulus of the strengthened soil. With growing ES from 20 to 35 MPa, a sudden change occurs in the magnitude of horizontal shifts. Moreover, for ES ≥ 35 MPa, the distance between the curves becomes smaller, and for ES ≥ 50 MPa, the reduction in horizontal shifts is limited to a maximum of 11 mm.

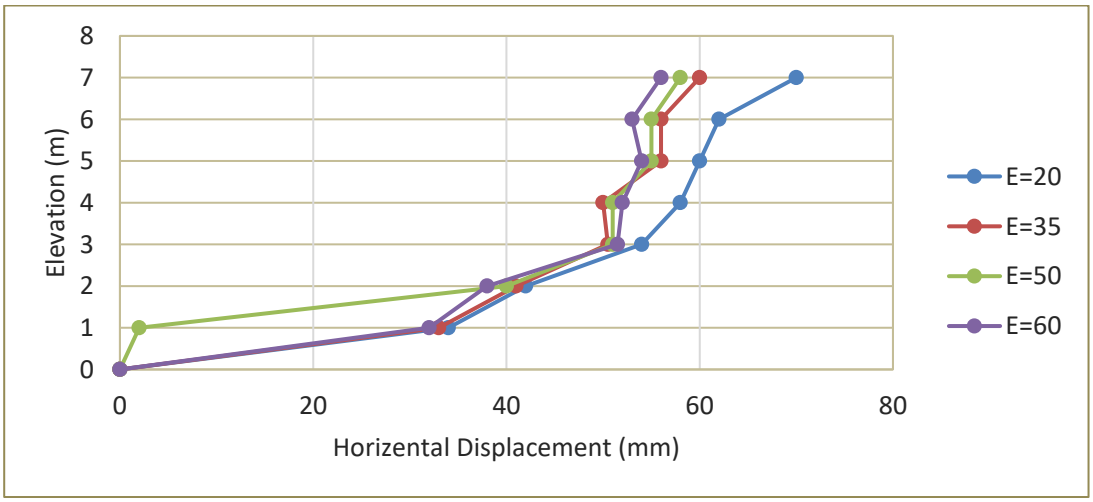

Fig. 16 - Effect of the elastic modulus of the strengthened soil on the horizontal shift of the wall at the end of the 0.3 g base input acceleration

D) Vertical shift of the Top and Bottom of the Wall:

Figure 17 presents the vertical shifts at both the top and bottom sections of the wall across diverse elastic modulus values. Elevating the elastic modulus of the strengthened soil results in reduced vertical shift at the wall's top. The maximum value observed is 9 mm for ES values greater than or equal to 35 MPa. Simultaneously, the vertical shift at the wall's bottom remains constrained within a maximum of 11.8 mm for elastic modulus values ranging from 20 to 35 MPa. Negligible changes are discernible for ES values exceeding 35 MPa. In summation, an upsurge in the elastic modulus of the strengthened soil has minimal impact on the vertical shifts at both the top and bottom of the wall.

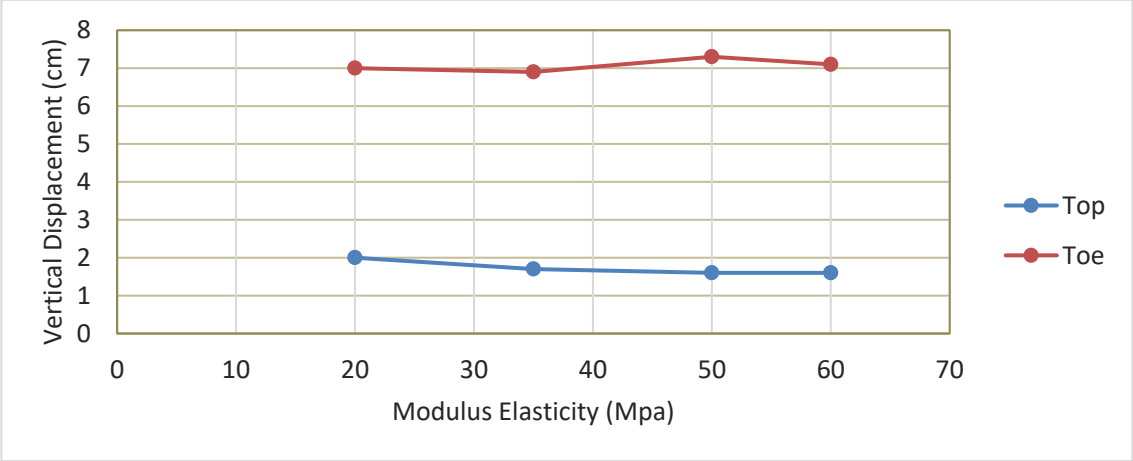

Fig. 17 - Effect of the elastic modulus of the strengthened soil on the vertical shifts of the top and bottom of the wall at the end of the 0.3 g base input acceleration

The impact of the Poisson's Ratio on the Strengthened soil

This section explores the impact of Poisson's ratio of the strengthened soil on the reaction of the strengthened soil structure.

A) Highest pulling Force of Reinforcements:

Figure 18 displays the fluctuation of the highest pulling force of reinforcements with height for diverse values of Poisson's ratio of the strengthened soil (PR). These curves indicate that the alteration in the value of Poisson's ratio has no significant impact on the increase or decrease in the highest pulling force of the reinforcements.

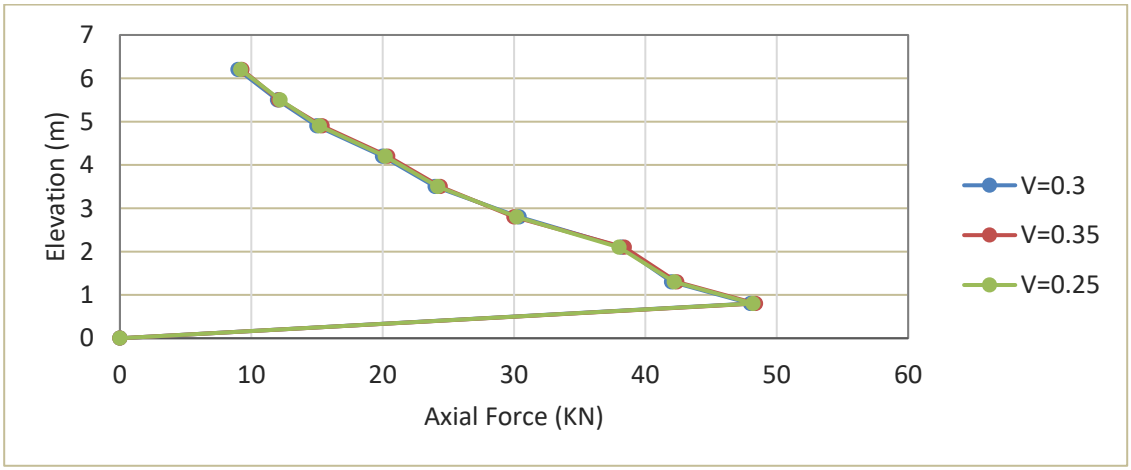

Fig. 18 - Effect of the Poisson's ratio of the strengthened soil on the highest pulling force of reinforcements at the end of the 0.3 g base input acceleration

B) Horizontal Pressure on the Rear of the Wall:

Figure 19 illustrates the impact of the change in Poisson's ratio on the horizontal pressure on the rear of the wall. As displayed in the figure, the change in Poisson's ratio has no crucial impact on the pressure.

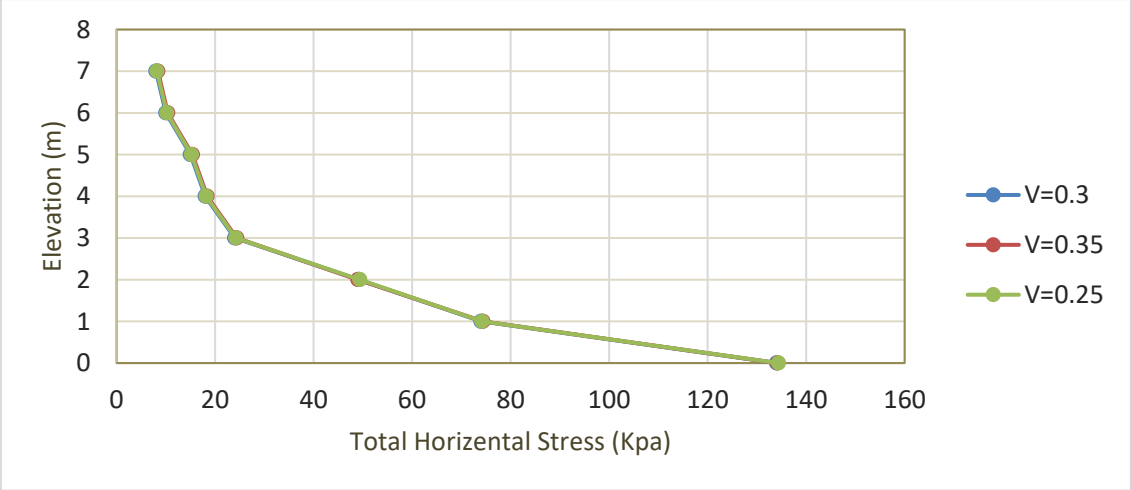

Fig. 19 - Effect of the Poisson's ratio of the strengthened soil on the horizontal pressure on the rear of the wall at the end of the 0.3 g base input acceleration

C) Horizontal Shift of the Wall:

Figure 20 displays the variation of horizontal shifts of the wall with height for diverse values of Poisson's ratio of the strengthened soil. Increasing the elastic modulus of the strengthened soil results in a slight escalation in the horizontal shifts, with the maximum escalation limited to 2.7 mm at a height of 7 meters of the wall.

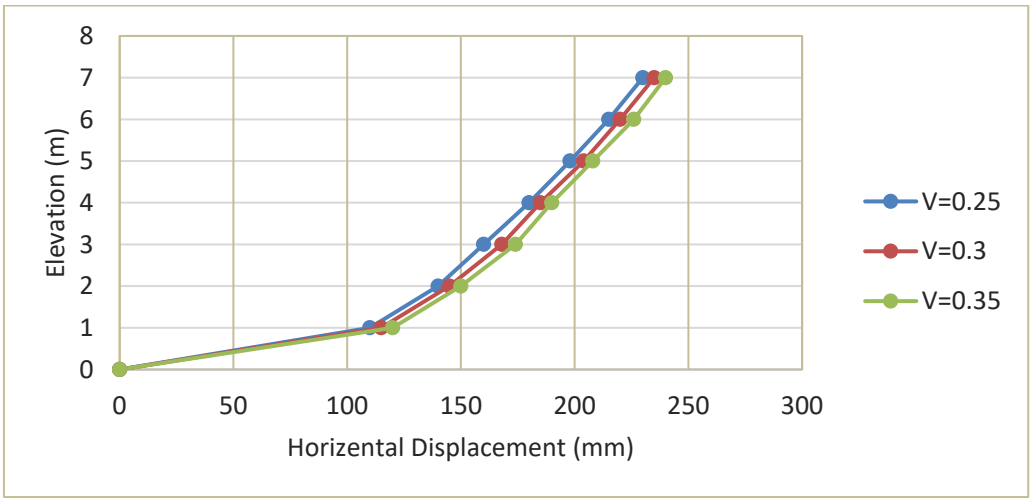

Fig. 20 - Effect of the Poisson's ratio of the strengthened soil on the horizontal shift of the wall at the end of the 0.3 g base input acceleration

D) Vertical Shift of the Top and Bottom of the Wall:

Figure 21 displays the vertical shift curves for diverse values of Poisson's ratio of the strengthened soil. The change in Poisson's ratio has no crucial impact on the vertical shifts of the top and bottom of the wall.

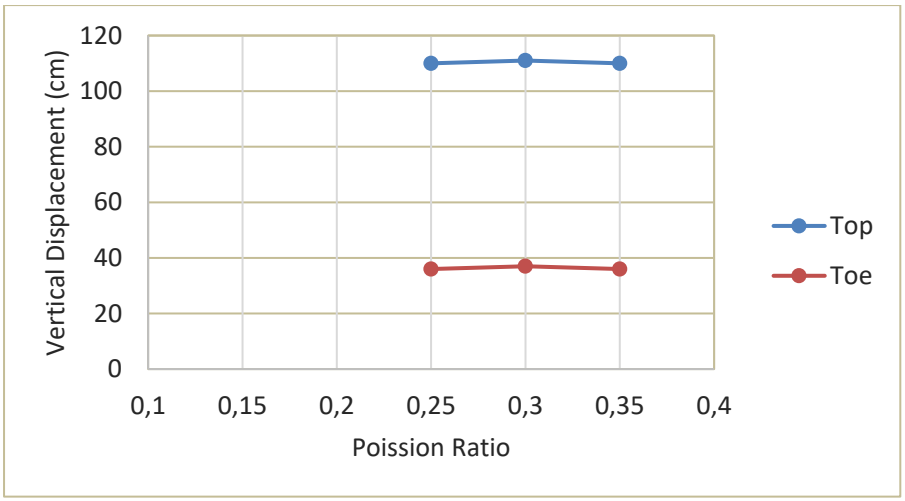

Fig. 21 - Effect of the Poisson's ratio of the strengthened soil on the vertical shifts of the top and bottom of the wall at the end of the 0.3 g base input acceleration

CONCLUSION

This research explores the seismic reaction of geogrid-strengthened soil walls through a comprehensive study of various influencing factors. The study focuses on assessing the impacts of parameters including adhesion, internal friction angle, elastic modulus, and Poisson's ratio on the execution of these structures under seismic loading states. By analyzing vertical and horizontal shifts, maximum pulling forces in reinforcing bars, and horizontal pressure on the wall's rear surface, this study provides insights into optimizing the structure and execution of geogrid-strengthened soil walls for seismic resilience.

- Seismic loading predominantly affects the lower half of the wall, necessitating stronger reinforcing bars in this section and leading to a significant increase in horizontal deformation compared to static states.
- Increasing adhesion values up to c = 10 kp effectively mitigate maximum pulling forces and horizontal pressure on the wall's rear surface. Beyond c = 40 kp, maximum pulling forces across reinforcing bars stabilize at various heights.
- Higher adhesion values (c ≥ 20 kp) consistently reduce horizontal deformation, suggesting a minimum adhesion requirement for controlling seismic-induced deformations.
- Elevating the internal friction angle (φ ≥ 39°) reduces maximum pulling forces in reinforcing bars, horizontal pressure on the wall, and horizontal deformation, contributing to optimal deformation control.
- Changes in elastic modulus (E ≥ 35 MPa) have minimal impact on maximum pulling forces but significantly reduce horizontal deformation, making soil with E ≥ 35 MPa advisable for horizontal deformation control.
- Alterations in Poisson's ratio do not significantly influence the studied parameters—maximum pulling forces in reinforcing bars, horizontal pressure on the wall, and horizontal and vertical deformations.

REFERENCES

[1]. Bao Y, Hu H, Gan G (2023) Seismic response analysis of slope reinforced by pile-anchor structures under near-fault pulse-like ground motions. Soil Dynamics and Earthquake Engineering 164:107576

[2]. Nunes GB, Portelinha FHM, Futai MM, Yoo C (2022) Numerical study of the impact of climate conditions on stability of geocomposite and geogrid reinforced soil walls. Geotextiles and Geomembranes 50:807–824

[3]. Yang K-H, Wu H-M, Tseng T-L, Yoo C (2023) Model tests of geosynthetic-reinforced soil walls with marginal backfill subjected to rainfall. Geotextiles and Geomembranes 51:342–359
[4]. Xu P, Hatami K, Jiang G (2020) Study on seismic stability and performance of reinforced soil walls using shaking table tests. Geotextiles and Geomembranes 48:82–97
[5]. Huang C-C (2019) Seismic responses of vertical-faced wrap-around reinforced soil walls. Geosynth Int 26:146–163
[6]. Bathurst RJ, Hatami K (1998) Seismic response analysis of a geosynthetic-reinforced soil retaining wall. Geosynth Int 5:127–166
[7]. Geng M (2021) A short review on the dynamic characteristics of geogrid-reinforced soil retaining walls under cyclic loading. Advances in Materials Science and Engineering 2021:1–10
[8]. Changizi F, Razmkhah A, Ghasemzadeh H, Amelsakhi M (2022) Behavior of geocell-reinforced soil abutment wall: A physical modeling. Journal of Materials in Civil Engineering 34:04021495
[9]. Holtz RD (2017) 46th Terzaghi lecture: geosynthetic reinforced soil: from the experimental to the familiar. Journal of Geotechnical and Geoenvironmental Engineering 143:03117001
[10]. Leshchinsky D, Han J (2004) Geosynthetic reinforced multitiered walls. Journal of Geotechnical and Geoenvironmental Engineering 130:1225–1235
[11]. Segrestin P, Bastick MJ (1988) Seismic design of reinforced earth retaining walls-the contribution of finiteelements analysis. In: International geotechnical symposium on theory and practice of earth reinforcement. pp 577–582
[12]. Zhang, R., Jiang, Y., & Zhang, Z. (2020). Numerical modeling of seismic behavior of reinforced soil walls considering soil-structure interaction. Soil Dynamics and Earthquake Engineering, 139, 106347.
[13]. Ling, H. I., & Leshchinsky, D. (2023). Contributions of physical modeling and numerical analysis to seismic behavior of reinforced soil retaining structures. In *Smart Geotechnics for Smart Societies* (pp. 72-91). CRC Press.
[14]. Ren, F., Huang, Q., Zhang, F., & Wang, G. (2024). Numerical study on seismic performance of tiered reinforced soil retaining walls. *Soil Dynamics and Earthquake Engineering*, *181*, 108672.
[15]. Majumder, M., Venkatraman, S., Bheda, M., & Patil, M. (2023). Numerical Studies on the Performance of Geosynthetic Reinforced Soil Walls Filled with Marginal Soil. *Indian Geotechnical Journal*, *53*(4), 805-826.
[16]. Javdanian H, Goudarzi N (2023) Seismic Analysis of Geogrid-Reinforced Soil Retaining Walls Under Decomposed Earthquake Records. Iranian Journal of Science and Technology, Transactions of Civil Engineering 1–13
[17]. Zhou L, Ding G (2021) Seismic response of reinforced retaining walls with saturated calcareous sand backfill subjected to acid rain erosion. Journal of Materials in Civil Engineering 33:06021005
[18]. Fairless GJ (1989) Seismic performance of reinforced earth walls
[19]. Murali Krishna A, Madhavi Latha G (2009) Seismic behaviour of rigid-faced reinforced soil retaining wall models: reinforcement effect. Geosynth Int 16:364–373
[20]. Safaee AM, Mahboubi A, Noorzad A (2023) Seismic behavior of tiered geogrid reinforced soil (GRS) using treated backfill soil. Geosynth Int 30:200–224
[21]. Qian Y (2023) Maximum dry unit weight and optimum moisture content prediction of lateritic soils using regression analysis. Advances in Engineering and Intelligence Systems 2:
[22]. Sadighi, H., Badiei, E., & Eslami Haghighat, A. (2022). Rational selection of pseudostatic seismic coefficient of slopes. *Iranian Journal of Science and Technology, Transactions of Civil Engineering*, *46*(6), 4529-4541.